Emergence of synchronization and regularity in firing patterns in time-varying neural hypernetworks

Sarbendu Rakshit,[1] Bidesh K. Bera,[1] Dibakar Ghosh,[1,*] and Sudeshna Sinha[2,†]
[1]*Physics and Applied Mathematics Unit, Indian Statistical Institute, 203 B. T. Road, Kolkata 700108, India*
[2]*Indian Institute of Science Education and Research Mohali, Manauli P.O. 140 306, Punjab, India*

(Received 27 December 2017; published 11 May 2018)

We study synchronization of dynamical systems coupled in time-varying network architectures, composed of two or more network topologies, corresponding to different interaction schemes. As a representative example of this class of time-varying hypernetworks, we consider coupled Hindmarsh-Rose neurons, involving two distinct types of networks, mimicking interactions that occur through the electrical gap junctions and the chemical synapses. Specifically, we consider the connections corresponding to the electrical gap junctions to form a small-world network, while the chemical synaptic interactions form a unidirectional random network. Further, all the connections in the hypernetwork are allowed to change in time, modeling a more realistic neurobiological scenario. We model this time variation by rewiring the links stochastically with a characteristic rewiring frequency f. We find that the coupling strength necessary to achieve complete neuronal synchrony is lower when the links are switched rapidly. Further, the average time required to reach the synchronized state decreases as synaptic coupling strength and/or rewiring frequency increases. To quantify the local stability of complete synchronous state we use the Master Stability Function approach, and for global stability we employ the concept of basin stability. The analytically derived necessary condition for synchrony is in excellent agreement with numerical results. Further we investigate the resilience of the synchronous states with respect to increasing network size, and we find that synchrony can be maintained up to larger network sizes by increasing either synaptic strength or rewiring frequency. Last, we find that time-varying links not only promote complete synchronization, but also have the capacity to change the local dynamics of each single neuron. Specifically, in a window of rewiring frequency and synaptic coupling strength, we observe that the spiking behavior becomes more regular.

DOI: 10.1103/PhysRevE.97.052304

I. INTRODUCTION

Naturally occurring systems typically interact with each other in different ways, with the nature of the links depending on the underlying coupling mechanism. In fact, different interwoven connection networks ensure proper functioning of such large interactive systems. From the dynamical perspective, different classes of interactions can be organized into distinct network structures. So within the network, a set of nodes may interact with a subset of other nodes through different types of interactions, and such networks are called *hypernetworks* [1]. Here multiple layers are formed by various interaction schemes among pairs of nodes, and these interactions are completely independent. So the presence of an edge between two specific nodes in one layer is independent of their connection in the other layers. Such hypernetworks have been used to mimic various complex phenomena, such as social interactions in multiplex networks [2], where inter- and intralayer connections are present simultaneously. The interdependent network, where nodes of each layer relay the information to nodes of the other layer for normal functioning, is exemplified by the coupled operation of power grid networks [3], transportation networks [4], and computer communication networks [3]. This concept is also seen in "networks of networks" [5] where connections between nodes belong to different networks. For instance, in coordinating their motion in shoals, fish not only use visual perception cues, but also release chemical signals in order to locate their mates in the shoal [6,7]. Another illustrative example is brain functions, which rely on interneuronal communications which take place through electrical gap junctions and chemical synapses simultaneously [8,9]. The interplay between the nodal dynamics and the structural properties of the connections of such coexisting independent networks can lead to highly nontrivial collective phenomena which have great relevance in biological, physical, technological, environmental, and social systems.

Few studies so far have focused on hypernetworks. Sorrentino [1] studied the synchronization dynamics and obtained the necessary and sufficient condition of synchronous states for low-dimensional hypernetworks where dimension was reduced by simultaneous block diagonalization of matrices of the network [10]. Sevilla-Escoboza *et al.* [11] studied the stability of enhancing synchrony in multivariable coupled oscillators in the network. The finite-size-induced transitions to synchrony in a network of phase oscillators [12] were investigated using nonlinear mean field interaction, where the prescribed network represented a fully connected hypernetwork structure at the microscopic level. Ouchi *et al.* [13] found different types of dynamical states in a coupled map lattice model in the presence of both local and global coupling, and

*dibakar@isical.ac.in
†sudeshna@iisermohali.ac.in

classified the pattern dynamics through characteristics such as the shape of the domains, distribution functions, power spectra, and degree of chaotic motion. In Ref. [14] the stability of synchronized states in networks of multiple communicating layers was analyzed through the master stability function approach.

Most existing studies have considered static hypernetworks where the underlying connection type and connection topology do not evolve over time. However, many real-life networks are not time invariant, i.e., the underlying network is not static. Rather, they are dynamically structured with the interactions appearing, disappearing, or rewired at different timescales [15]. Such time-varying features are seen in social interaction networks [16], where the relationship between pairs of individual social units change in a way such that the link between them can be continuously created or terminated over time. The temporal progression of links is an inherent feature of several natural and artificial networks, and a static approximation is valid only at large timescales [17]. In this context much attention has been devoted to studying the synchronization phenomena in time-varying complex networks [18–24]. The collective features emerging in time-varying systems have wide applicability in various fields, including consensus problems [25], disease spreading [26], functional brain networks [27], power transmission systems [28], person-to-person communication [29], the process of chemotaxis [30], wireless sensor networks [31], and many biological networks like metabolism, protein-protein interaction, and gene-regulatory networks [32].

In neuronal systems, one neuron is connected to another neuron through a synaptic connection to perform several biological functions. Importantly, existing neuronal interactions may not be active for all time, and new links may form over time. This makes the framework of temporal networks most suitable for modeling neuronal communication, as the passage of chemical molecules and electrical signals between neurons can be mimicked by a temporary edge between them that is switched "on" when these flows are active [15]. There have been few studies incorporating the time-varying character of connections in this context [27,33,34]. So the shift from static to dynamic neuronal interaction is essential for further understanding of neuronal communication. Previously, Bassett *et al.* [35] discussed the structure of functional brain networks, and very recently they revisited [36] the small-world property of the brain network, recapitulating that the graphical representation of the nervous system of *C. elegans* obtained experimentally shows small-world topological organization. The question of brain networks adhering to small-world patterns was also recently considered in Ref. [37].

Inspired by the above, in this work, we consider a large neuronal network where the dynamics at each node is modeled by Hindmarsh-Rose neuronal oscillators, and the coupling between the neurons arises through electrical and chemical synapses. As electrical gap junctional coupling is bidirectional and the chemical synaptic interaction is unidirectional in nature, we will consider the former type of coupling to belong to a small-world network and the latter type to belong to a unidirectional random network. The coexistence of both types of networks within one network constitutes a hypernetwork. Further, since the connection between neurons through synapses is highly dynamic, we will consider the links to be rewired over time with a characteristic rewiring frequency.

With the above time-varying neuronal hypernetwork, we will focus on the emergence and stability of complete neuronal synchronization. While complete synchrony has been found to arise in networks consisting of neuronal connections of one particular type, here we will explore the emergence of synchrony in the presence of both types of synaptic interactions, constituting different connection topologies. Further, since we consider time-varying hypernetworks, we will explore the role played by the timescale of switching links on neuronal synchrony. In addition to synchrony, we will also search for significant changes in the firing patterns of the individual neurons that may arise due to the variations in the links of the hypernetwork. Our basic aim here is to shed light on emergent phenomena in time-varying hypernetworks through the illustrative example of this model hypernetwork inspired by broad features of neuronal systems interacting through both electrical and chemical synapses.

We will use two approaches to characterize temporal patterns in the hypernetwork. The first approach will be through linear stability theory, which provides a measure of the local stability of systems under small perturbations around the synchronization manifold. Through this stability analysis, we will derive the necessary condition for the complete neuronal synchrony. In addition to the usual linear stability approach, we will explore the global stability of the network against large perturbations, which are omnipresent in nature. Since the conditions obtained from linear stability analysis are necessary but not sufficient, we will use the concept of basin stability (BS) [38] for the quantification of the global stability of the neuronal hypernetwork. BS is a nonlocal, nonlinear measure that relates to the volume of the basin of attraction of a dynamical state. BS is easily applicable to high-dimensional complex systems and is an important extension to the traditional linearized approach to understanding dynamical stability. It is especially useful in the study of multistable systems with coexisting dynamical attractors and has been used to characterize coupled delayed [39] and nondelayed systems [40], synchronized states [41], and coexistence of synchronous and desynchronous states [42,43]. In addition to linear stability analysis and estimation of basin stability, we will also find the mean time required to reach the synchronized state from generic random initial states and use this quantity to demonstrate that the time taken to approach the synchronized state is shortened significantly in networks where the links are rapidly rewired and/or synaptic coupling is stronger. Finally, we will investigate the firing regularity of the individual neurons in our neuronal hypernetwork by calculating the interspike interval (ISI) and the corresponding the coefficient of variation (CV), focusing on the effect of the time-varying nature of the connections on the local dynamics (i.e., the firing pattern of the single neuron).

II. GENERAL MATHEMATICAL MODEL FOR TIME-VARYING HYPERNETWORKS

We start by considering a network composed of N nodes and M different interacting layers. Each node represents a d-dimensional dynamical system, where the state vector of the ith node is described by a vector $\mathbf{x}_i$, and the corresponding evolution function $F(\mathbf{x}_i)$ is continuously differentiable. The interaction function between the ith and jth nodes in the layer

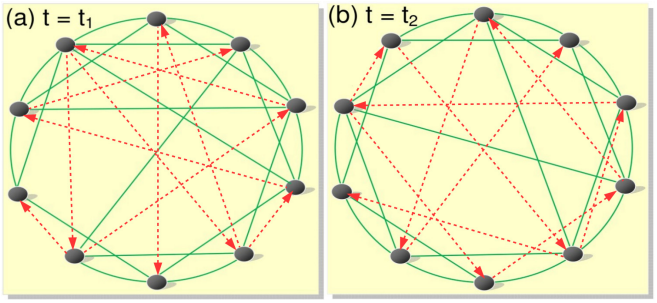

FIG. 1. Schematic representation of time-varying connections in a hypernetwork at two different time instants: (a) t_1 and (b) t_2. Each node is denoted by a gray solid circle. The red dashed lines denote unidirectional interactions and form a random network with constant in-degree 1, while the green solid lines represent bidirectional coupling, forming a small-world network of average degree 4.

l is denoted by $H_l(\mathbf{x}_i,\mathbf{x}_j)$, which belongs to the C^1 vector field. Then the mathematical equation of the time-varying hypernetwork is written as

$$\dot{\mathbf{x}}_i = F(\mathbf{x}_i) + \sum_{l=1}^{M} \epsilon_l \sum_{j=1}^{N} \mathscr{A}_{ij}^{(l)}(t) H_l(\mathbf{x}_i,\mathbf{x}_j), \quad i = 1,2,\ldots,N, \tag{1}$$

where ϵ_l is the layer-dependent coupling strength. Here $\mathscr{A}^{(l)}(t)$ is the adjacency matrix of the lth layer at time t, whose elements are $\mathscr{A}_{ij}^{(l)}(t) = 1$ if ith and jth nodes are connected at that particular time t and 0 otherwise. Adjacency matrices $\mathscr{A}^{(l)}(t)(l = 1,2,\ldots,M)$ may be symmetric or asymmetric depending on whether the underlying network of the layer l is bidirectional or unidirectional. At any time t, each link in the network is rewired with probability $f\,dt$, where dt is the integration time step and f is the rewiring frequency; i.e., at each time step the existing network is replaced by a new network with probability $f\,dt$. So at each time step, the adjacency matrix $\mathscr{A}^{(l)}(t)$ of each layer changes. Large f implies that the networks are changing rapidly, whereas a low value of f indicates that the networks are almost static.

A schematic diagram illustrating time-varying interactions in such a hypernetwork of $N = 10$ nodes and $M = 2$ layers is shown in Fig. 1. By considering the distinct nature of the interaction, we construct two different types of interacting layers, one a unidirectional random network and other one a bidirectional small-world network. The green solid line shows a small-world network of average degree 4 corresponding to the bidirectional coupling, and the dashed red line shows the unidirectional random network with constant in-degree 1. The coexistence of these two networks constitute a hypernetwork, with each layer generally having different links and representing a different kind of interaction. At two particular instances of time $t = t_1$ and $t = t_2$, the different interaction patterns, as reflected by different links, are shown in Figs. 1(a) and 1(b), respectively.

III. APPLICATION OF THE MATHEMATICAL FRAMEWORK TO A MODEL NEURONAL NETWORK

A neuronal network may be modeled by time-varying hypernetworks, as neurons interact through both electrical gap junctions, as well as chemical synapses, and these links are known to vary with time. These two types of synapses are elementary functional connections which enable information to be swiftly transferred between neurons. Through a chemical synapse, a signal is conveyed chemically via neurotransmitter molecules such as acetylcholine, gamma-aminobutyric acid, dopamine, and serotonin, packaged inside small synaptic vesicles. In a probabilistic manner neurotransmitters are released by exocytosis from a presynaptic neuron into the synaptic cleft. These molecules then bind to specific postsynaptic receptors in adjacent postsynaptic neuronal cells, leading to a unidirectional transmission of information. In this case, the distance between pre- and postsynaptic ends may be large, approximately 20–40 nm [44].

In electrical synapses the cytoplasm of adjacent cells is directly connected by a channel called a gap junction. So direct bidirectional passage of electric current, calcium, cyclic AMP, and inositol-1,4,5 trisphosphate occurs between the presynaptic end and the postsynaptic neuron. Here the membranes of the pre- and postsynaptic neurons are extremely close to each other, approximately 3.5 nm [45]. So electrical synapses are naturally bidirectional, and the signal transmission speed is much faster than chemical transmission.

Both these types of synapses coexist in most nervous systems. For interneuronal communication both types of coupling are not necessarily present simultaneously, rather they operate independently [46] over time. The coexistence of chemical and electrical synapses among two neurons is known as a mixed synapse, while heterosynaptic interaction is a neuron connected with two different neurons, one by a chemical synapse and another by an electrical synapse.

Here each node of the network is modeled through Hindmarsh-Rose (HR) neuronal systems whose velocity profile is described by $F(\mathbf{x}) = \{y - ax^3 + bx^2 - z + I, c - dx^2 - y, r[s(x - x_0) - z]\}^T$. Considering two ($M = 2$) synaptic interaction layers as $H_1(\mathbf{x_i},\mathbf{x_j}) = [(v_s - x_i)\Gamma(x_j),0,0]^T$ and $H_2(\mathbf{x_i},\mathbf{x_j}) = [x_j - x_i,0,0]^T$ with corresponding coupling strengths $\epsilon_1 = g_c$ and $\epsilon_2 = \epsilon$, where T denotes transpose of a matrix. Here H_1 and H_2 represent the mathematical forms of the chemical and electrical coupling functions, respectively. Therefore, the dynamics of such a neuronal time-varying hypernetwork is described by the set of equations

$$\begin{aligned}
\dot{x}_i &= y_i - ax_i^3 + bx_i^2 - z_i + I \\
&\quad + \frac{g_c}{k_c}(v_s - x_i)\sum_{j=1}^{N} \mathscr{A}_{ij}^{(c)}\Gamma(x_j) - \epsilon \sum_{j=1}^{N} \mathscr{L}_{ij}^{(e)} x_j, \\
\dot{y}_i &= c - dx_i^2 - y_i, \\
\dot{z}_i &= r[s(x_i - x_0) - z_i],
\end{aligned} \tag{2}$$

where $i = 1,2,\ldots,N$ is the neuron index, x_i is the membrane potential of the ith neuron, y_i is associated with the fast current, for example, Na^+ or K^+, and z_i with the slow Ca^{2+} current, where r modulates the slow dynamics of the system. Strengths of the chemical and electrical coupling are g_c and ϵ, respectively, and these determine how the information is distributed between neurons through the different coupling channels. We consider parameters $a = 1, b = 3, c = 1, d = 5, r = 0.005, s = 4, x_0 = -1.6, I = 3.25$, for which the

isolated system exhibits multitimescale chaotic behavior of the membrane potential, known as spiking bursting.

Interneuronal communication in the brain relies on information transmission, which happens principally through two types of interactions that operate independently and may coexist during information processing [46]: bidirectional electrical gap junctional coupling and the unidirectional chemical ion transportation through chemical synapses. So in our hypernetwork structure mimicking neuronal networks, the connectivity of the chemical synapses is considered to be a unidirectional random network, described by the adjacency matrix $\mathscr{A}^{(c)}$. The corresponding Laplacian matrix is given by $\mathscr{L}^{(c)}_{ij} = -\mathscr{A}^{(c)}_{ij}$ for $i \neq j$, and $\mathscr{L}^{(c)}_{ii} = \sum_{j=1}^{N} \mathscr{A}^{(c)}_{ij}$. We consider identical in-degree k_c of each node (as diverse in-degree of the nodes does not yield complete synchronization due to the absence of the synchronization manifold). Hence the average in-degree of our network is $\langle k_c \rangle = k_c$, which reflects the number of signals each neuron receives through chemical synapses. In this unidirectional random network, if there is an edge from node i to j, it will be rewired from node i to any another node excluding j with probability $(1 - \frac{k_c}{N-1})fdt$. The mechanism for the activation and deactivation of a nonlinear chemical synapse is modeled by the sigmoidal input-output function $\Gamma(\mathbf{x}) = \frac{1}{1+\exp[-\lambda(\mathbf{x}-\Theta_s)]}$. The synaptic reversal potential is v_s, and for $v_s > x_i(t)$ the synaptic current has a depolarizing effect making the synapse excitatory, and for $v_s < x_i(t)$ the synaptic current has a hyperpolarizing effect making the synapse inhibitory. For the chosen set of system parameters, $|x_i(t)| < 2$, thus $[x_i(t) - v_s]$ is always negative if $v_s = 2$, and so that the chemical synapse is excitatory forever, i.e., when the presynaptic neuron spikes, it induces the postsynaptic neuron to spike. The parameter λ determines the slope of the sigmoidal function, and Θ_s is the synaptic firing threshold. Hereafter $\Theta_s = -0.25$ and $\lambda = 10$. We consider the electrical synaptic network to have a small-world structure [35,47–49], constructed by a Watts-Strogatz (WS) network algorithm [50], whose Laplacian matrix is denoted by $\mathscr{L}^{(e)}$. This is a zero row sum matrix with average degree $\langle k_e \rangle$. In this small-world network, if the edge is between two distant neighbors, it is rewired to a nearest neighbor of one of the nodes with probability $(1 - p)fdt$, and if the edge is between two nearest neighbors, then with probability $pfdt$, it is replaced by a connection to a randomly chosen distant node.

IV. RESULTS

We integrate the dynamical equations of this hypernetwork [cf. Eq. (2)] numerically by the fifth-order Runge-Kutta method. Specifically, we consider a network consisting of $N = 200$ neurons and follow the system over 3×10^5 time steps, using an integration time step of 0.01. We calculate the synchronization error defined as

$$E = \left\langle \frac{1}{N-1} \sum_{j=2}^{N} \sqrt{(x_j - x_1)^2 + (y_j - y_1)^2 + (z_j - z_1)^2} \right\rangle_t, \tag{3}$$

where $\langle \cdot \rangle_t$ is the time average obtained over a large time interval (taken as 1×10^5 time steps). Complete neuronal synchronization corresponds to the case when all neurons follow the same trajectory and yields zero synchronization error.

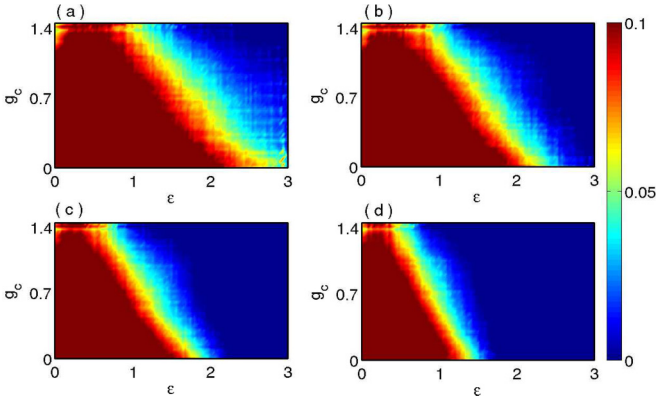

FIG. 2. Synchronized and desynchronized regions in the (ϵ, g_c) parameter space for different rewiring frequencies: (a) $f = 0.001$, (b) $f = 0.01$, (c) $f = 0.1$, and (d) $f = 1.0$. The color bar represents the value of the synchronization error defined in the text. The other parameters in the system are fixed at $p = 0.1, k_c = 5, k_e = 6$.

Note that in this work our central aim is to understand the influence of network structure on the synchronization and firing patterns in a hypernetwork of chaotic neuronal oscillators. So we keep the local parameters of the individual HR model neurons fixed in the chaotic bursting mode and focus our investigation on the subset of parameters directly related to network structure and coupling function. In what follows we will explore the spatiotemporal dynamics under variation of parameter p reflecting the randomness of the links, parameter f reflecting the time-varying nature of the links, and parameters ϵ and g_c giving the comparative strengths of the electrical and chemical coupling.

Figure 2 shows the synchronization error in the space of electrical and chemical synaptic coupling strengths (ϵ, g_c), for rewiring frequencies f ranging from 0.001 to 1.0. Note that in a network of neurons the links may change at different rates depending on factors such as environmental stimuli and the developmental stage of the network. Thus it is important to investigate a large range of rewiring frequencies f. Typically though the rewiring rates are expected to be low in realistic situations, and so the simulations at $f \sim 0.01$–0.001 are likely to be most relevant to a neuronal network.

It is evident from Fig. 2(a) that the region in (ϵ, g_c) parameter space where complete synchronization occurs (shown in deep blue) enlarges with increasing f. This implies that *more rapidly changing networks yield larger windows of complete synchronization in the parameter space of the electrical and chemical coupling strengths*. It is also evident from this figure that complete synchrony is impossible in the absence of coupling through chemical synapses (i.e., $g_c \sim 0$) for low rewiring frequencies. However, it is clear from Figs. 2(c) and 2(d) that for sufficiently high rewiring frequency, neuronal synchrony emerges even in the absence of chemical coupling. The critical electrical gap-junction coupling ϵ^* needed for synchrony in the absence of chemical coupling decreases with increasing rewiring frequency, e.g., it is $\sim$2.43 for $f = 0.01$ and $\sim$1.83 for $f = 1$. As the strength of chemical coupling

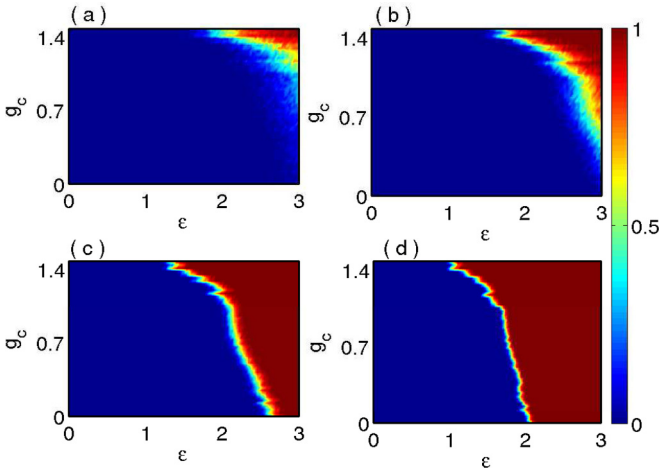

FIG. 3. The BS corresponding to the Fig. 2 for various rewiring frequencies: (a) $f = 0.001$, (b) $f = 0.01$, (c) $f = 0.1$, and (d) $f = 1.0$. The other parameters in the system are fixed as in Fig. 2.

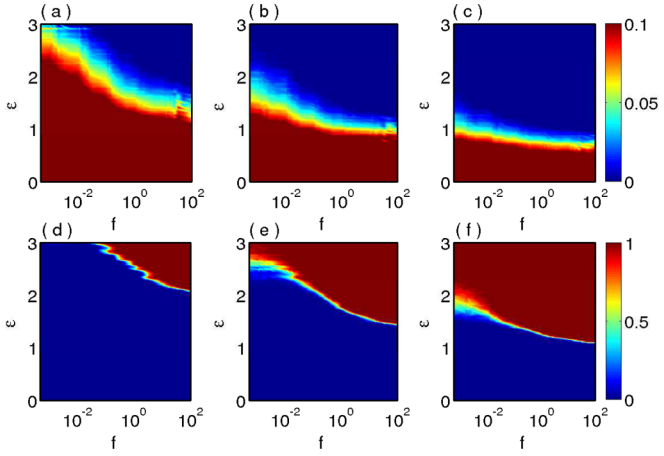

FIG. 4. Synchronization error (upper) and BS measure (lower) in the (f,ϵ) parameter space, for $k_e = 4$ (left), $k_e = 6$ (middle), and $k_e = 8$ (right). Other parameters in the system are fixed at $p = 0.1, k_c = 5, g_c = \frac{\epsilon}{2}$.

g_c increases, the critical value of ϵ decreases approximately linearly with g_c, i.e., $\epsilon^* \sim 1/g_c$ for fixed f. The presence of electrical coupling is more crucial to the emergence of complete synchronization, as no complete synchrony is possible for $\epsilon = 0$. The critical value of chemical coupling strength necessary to induce complete synchrony decreases with increasing electrical coupling strength, becoming zero at ϵ^*. So the presence of chemical coupling (i.e., $g_c \neq 0$) aids the onset of complete synchronization at lower electrical coupling strengths, and the strong presence of both types of interactions (i.e., high ϵ and high g_c) yields complete neuronal synchrony.

The global stability of the completely synchronous neuronal state is analyzed using basin stability (BS), defined as

$$\mathrm{BS} = \int_{\mathscr{B}} \chi(\mathbf{x})\rho(\mathbf{x})\, d\mathbf{x}, \tag{4}$$

where $\mathscr{B}$ is the set of all possible random perturbations $\mathbf{x}$ and $\chi(\mathbf{x})$ is equal to one if the system converges to synchronized states after perturbation $\mathbf{x}$ and zero otherwise. Here $\rho(\mathbf{x})$ is the density of the perturbed states with $\int_{\mathscr{B}} \rho(\mathbf{x})\, d\mathbf{x} = 1$. For numerical computation, we integrate the dynamical equations of the system for sufficiently large number (T) of random initial conditions drawn uniformly from a prescribed region of phase space. Let M be the number of initial conditions that finally arrive at the synchronous state. Then the BS for the synchronous state is estimated as $\frac{M}{T}$. BS is bounded in the range $[0,1]$. When $\mathrm{BS} = 0$, the synchronized state is completely unstable and has a basin of attraction approaching zero. When $\mathrm{BS} = 1$, all sampled initial states are attracted to the synchronized state, suggesting a globally attracting synchronized state. $0 < \mathrm{BS} < 1$ corresponds to the probability (in the classical sense) of getting the synchronous states for a random initial state lying within the prescribed region of phase space. Here we sample the phase space volume $[-1.5,2.0] \times [-7.0,1.0] \times [2.9,3.4]$, and the system is considered as synchronized if $E < 10^{-5}$.

The BS of the completely synchronous state is shown in (ϵ, g_c) parameter space in Fig. 3, corresponding to Fig. 2. The color bar shows the variation of BS. The deep blue area corresponds to $\mathrm{BS} \sim 0$ indicating that any randomly chosen initial condition gives rise to incoherent dynamics. The deep red are occurs where $\mathrm{BS} \sim 1$, signifying that the prescribed region of phase space fully supports the coherent state. The intermediate color indicates $0 < \mathrm{BS} < 1$, implying the coexistence of synchronized and desynchronized states. Figures 3(a)–3(d) show the BS for rewiring frequencies $f = 0.001, 0.01, 0.1, 1.0$ and correspond to those displayed in Figs. 2(a)–2(d). Comparison of these figures shows that the enlargement of the synchronous region with increasing f and the decrease in critical coupling strengths observed in Fig. 2 are clearly reflected in the BS measure as well; i.e., increasing either electrical or chemical coupling strengths increases the basin stability of the synchronous state. Interestingly, we also see that the region of coexistence of the synchronous and desynchronous states decreases as rewiring frequency increases. So for more static networks (i.e., with low f) the transition of the BS of the synchronous state from 0 to 1, with increasing coupling strength, is quite gradual. However, *for rapidly switched links there is a sharp transition from the incoherent to the synchronous state*.

We now systematically explore the dependence of the synchronization error and basin stability of the synchronous state on the coupling strength and rewiring frequency. The results are displayed in Fig. 4. The upper panel in Fig. 4 represents the synchronization and desynchronization region characterized by synchronization error, while the lower panel displays the global robustness of synchronous state in terms of BS. Three average degrees of the SW network, $k_e = 4, 6$, and 8, are shown, with the average in-degree of the chemical synaptic network fixed at $k_c = 5$ and coupling strength $g_c = \frac{\epsilon}{2}$. These figures clearly show that the synchronization region is smaller when the network has lower degree [cf. Fig. 4(a) *vis-à-vis* Figs. 4(b) and 4(c)]. These trends are also reflected in the BS measure [cf. Figs. 4(d) and 4(f)]. The critical value of coupling strengths necessary for the onset of synchrony decreases for increasing f. This effect is clearly discernible in lower degree networks, where rapid switching significantly aids synchronization. However, in higher degree networks the effect of dynamic rewiring is less prominent. This is

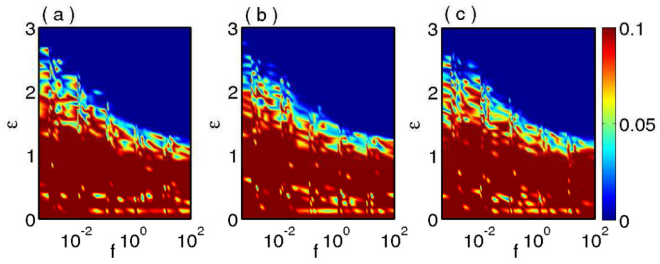

FIG. 5. Synchronization error in the (f,ϵ) parameter space. Here k_c is equal to (a) 2 (b) 4, (c) 6, and $k_e = 6$, $g_c = \epsilon/2$, $p = 0.1$.

understandable, as for a network approaching the globally connected limit, the variation of links will have no effect at all. Last, we note that the region of coexistence of the synchronous and desynchronous states again shrinks in rapidly changing networks.

Next we investigate the effect of varying average in-degree k_c in the random unidirectional network modeling the chemical synaptic connections, for fixed value of k_e. Figure 5 shows the effect of the number of chemical synaptic connections per neuron on the dynamics of the full network. It is clear that the qualitative behavior of the system remains quite unchanged under varying k_c.

Figure 6 shows the synchronization error in the upper panels and the BS of the synchronous state in the lower panels for varying p and ϵ. The average degree of the electrical synaptic network k_e is 4 in the left panels and 8 in the right panels. From these figures it is clear that higher average degree is more favorable for synchronization. This is intuitively obvious, as higher degree networks have a larger number of links on average, leading to more efficient information transmission. Further, it is evident that higher WS probability p aids synchronization. In the limit of $p \sim 1$, when the network tends to an Erdős-Rényi (ER) random network, complete synchrony occurs for chemical synaptic coupling strengths above a threshold. However, for low values of p ($p \sim 0$) there is no synaptic coupling strength that yields complete synchronization. These results

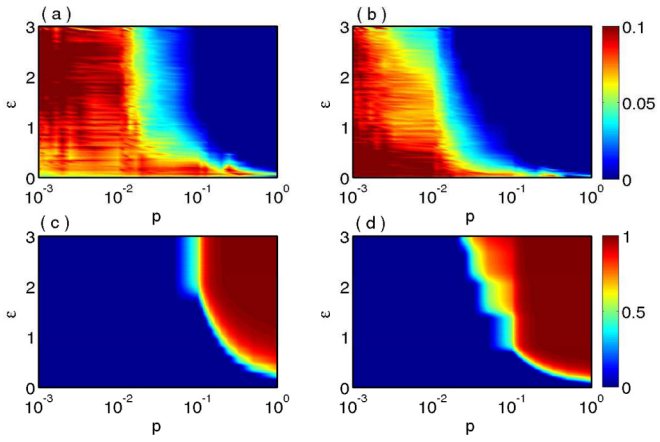

FIG. 6. Synchronization error (upper) and BS (lower) in the (ϵ, p) parameter space. The average degree of the WS network is $k_e = 4$ (left) and $k_e = 8$ (right). Average in-degree of the chemical synaptic network is $k_c = 5$ and chemical coupling strength $g_c = 1.4$.

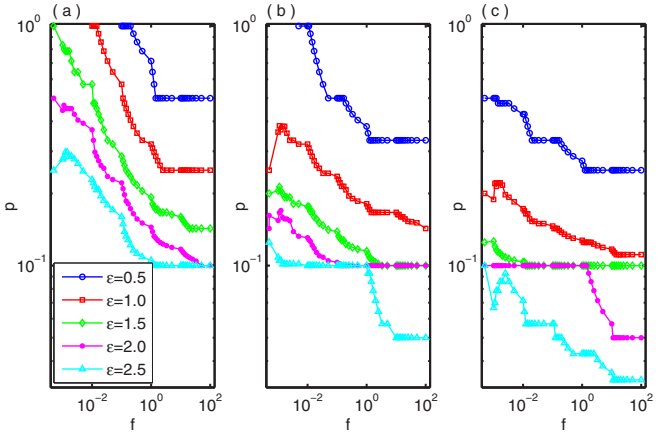

FIG. 7. Curves showing the boundary in (f,p) parameter space where the synchronization-desynchronization transition occurs. The region above the curves has synchronized states, and the region below has desynchronized states. The electrical synaptic network has different average degrees: (a) $k_e = 4$, (b) $k_e = 6$, and (c) $k_e = 8$. Here $k_c = 5$, $g_c = \frac{\epsilon}{2}$, and ϵ varies from 0.5 to 2.5.

are in concurrence with earlier observations that the range of synchronization is enhanced monotonically by increasing p in small-world networks, with ER random networks yielding the largest window of synchronized states [51–53].

Next we investigate the interplay of the WS probability p and rewiring frequency f on the emergence of neuronal synchrony in the hypernetwork. The curves in Fig. 7 demarcate the boundary of the synchronization-desynchronization transition in (f,p) parameter space. The area above the curves has synchronized states, and the region below has desynchronized states. The three panels in Fig. 7 correspond to different average degrees of the random network: $k_e = 4$, $k_e = 6$ and $k_e = 8$, respectively The figure reveals that increasing both f and p aids neural synchrony. So when the links switch very fast (i.e., f is high) and the chemical and electrical synaptic networks are both random (i.e., $p = 1$), it takes very low synaptic coupling strengths to synchronize the entire hypernetwork.

To gain a deeper understanding of the synchronization process we evaluate the average time taken to reach the synchronized state. This quantity is shown in Fig. 8, for several representative values of rewiring frequency f. We find that rapidly changing networks take much less time to reach synchronization. Further, synchronization time decreases with increasing synaptic coupling strengths.

Next we study the role of system size in the onset of neuronal synchrony in time-varying hypernetworks. This is relevant for the human brain, which consists of a very large number of neurons that interact through both electrical and chemical synapses. In order to gain insight into the effect of the size of the neuronal network on synchrony, we find the critical size, i.e., the critical number of nodes N^*, up to which complete neural synchrony is obtained. We then explore the dependence of N^* on coupling strength ϵ and rewiring frequency f, as displayed in Figs. 9(a) and 9(b), respectively. The parameter regions above and below each curve denote the desynchronized and synchronized states, respectively. It is clear that N^* increases with increasing coupling strength and rewiring frequency. So,

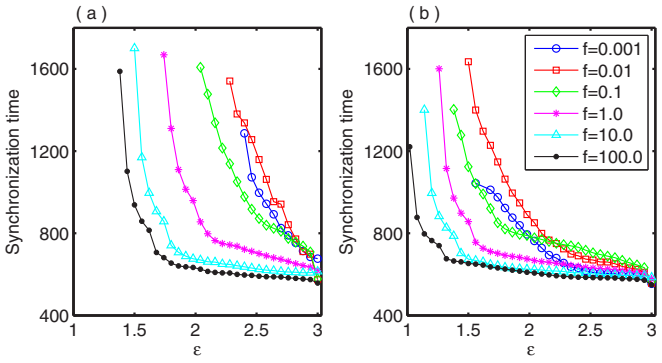

FIG. 8. Synchronization time for different coupling strengths and rewiring frequencies, where the average degree of the electrical synaptic small-world network is (a) $k_e = 6$ and (b) $k_e = 8$. The other system parameters are $k_c = 5, p = 0.1, g_c = \frac{\epsilon}{2}$.

while increasing the network size induces desynchronization, synchrony can be maintained up to larger network sizes N^* by increasing either synaptic strength or rewiring frequency. This trend can be rationalized as follows: if the number of nodes in a network is increased, with fixed average degree, then the probability of interaction between two fixed nodes decreases. So larger coupling strength and rewiring frequency are needed for the complete synchrony. *This implies that under rapid rewiring and strong coupling, much larger networks manage to remain in stable synchrony, and this observation may be relevant for the human brain, where the neuronal network size is very large.*

Last, we explore the dynamics of the hypernetwork where the rewiring rates of the two constituent networks are different; i.e., the rewiring frequencies of the chemical and electrical synaptic networks, denoted by f_c and f_e respectively, are

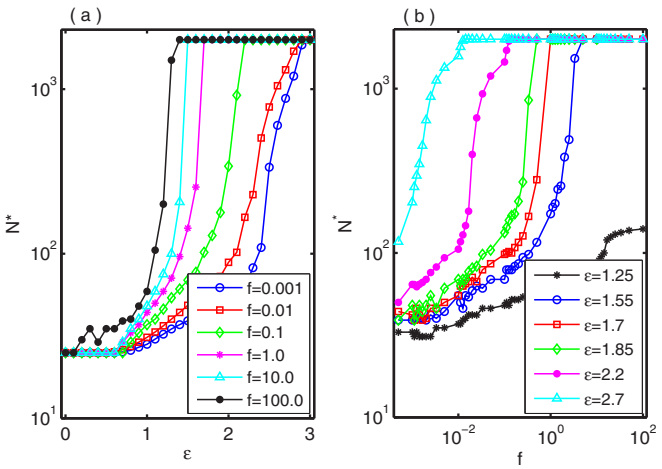

FIG. 9. Dependence of the critical number of nodes N^* up to which complete neural synchrony is obtained, on (a) coupling strength ϵ (for different fixed f) and (b) rewiring frequency f (for different fixed ϵ). The parameter regions above and below each curve denote the desynchronized and synchronized states, respectively. The other system parameters are $p = 0.1, k_e = 6, k_c = 5$, and $g_c = \frac{\epsilon}{2}$. Here we consider up to $N = 2000$. Note that we have checked that the qualitative features remain the same for larger N.

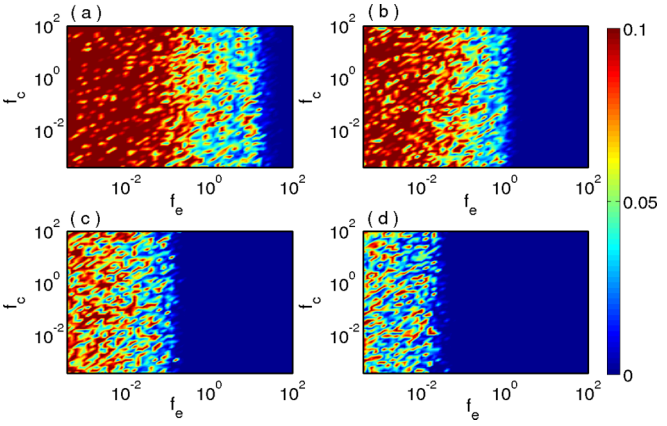

FIG. 10. Synchronization error in the (f_e, f_c) parameter space. Here f_e and f_c represent the rewiring frequencies of the small-world network modeling electrical synapses and the unidirectional random network modeling chemical synapses. The coupling strengths are (a) $\epsilon = 1.3$, (b) $\epsilon = 1.5$, (c) $\epsilon = 1.8$, (d) $\epsilon = 2.1$, and $k_e = 6$, $k_c = 5$, $p = 0.1$, and $g_c = \epsilon/2$.

not equal. Here we are motivated by the fact that typically the timescale of change of the different types of synaptic connections may be different, as the underlying coupling mechanisms are indeed different. We present in Fig. 10 the synchronization error arising in the hypernetwork for f_e and f_c varying over five orders of magnitude, with $f_e \neq f_c$ in general. Very interestingly, we find that the emergent synchronization is sensitive only to the rate at which the connection network of electrical synapses rewire. This suggests that in complex hypernetworks it may emerge that the *time dependence of one type of connection network primarily determines the full network dynamics.*

A. Linear stability analysis

We devote this section to the linear stability analysis of the synchronized state. We consider the time-varying network to be well approximated by a time-averaged static network, for sufficiently fast rewiring [18]. Let $\bar{\mathcal{A}}^{(c)}$ be the time-averaged adjacency matrix of the network of chemical synapses with $\sum_{j=1}^{N} \bar{\mathcal{A}}_{ij}^{(c)} = d_i^{(c)}$ and $\bar{\mathcal{D}}^{(c)} = \mathrm{diag}(d_1^{(c)}, d_2^{(c)}, \ldots, d_N^{(c)})$, and $\bar{\mathcal{L}}^{(c)}$&$\bar{\mathcal{L}}^{(e)}$, respectively, be the Laplacian matrices of the time-averaged network for the chemical and electrical synapses, with respective set of eigenvalues $\{0, \gamma_2^{(c)}, \ldots, \gamma_N^{(c)}\}$ and $\{0, \gamma_2^{(e)}, \ldots, \gamma_N^{(e)}\}$. Then there exists a constant T (sufficiently large) such that

$$\bar{\mathcal{L}}^{(c,e)} = \frac{1}{T} \int_t^{t+T} \mathcal{L}^{(c,e)}(\tau)\, d\tau, \tag{5}$$

with the time-averaged network and the rapidly varying network yielding the same synchronization transition, for sufficiently fast switching [54]. The entries of $\bar{\mathcal{L}}^{(e)}$ are $-(1-p)$ for nearest neighbors and $\frac{-2kp}{N-2k-1}$ for distant nodes, and $\bar{\mathcal{L}}_{ij}^{(c)} = \frac{-k_c}{N-1}$ for $i \neq j$ and $\bar{\mathcal{L}}_{ii}^{(c)} = k_c$ for $i, j = 1, 2, \ldots, N$. Hence the time-averaged system corresponding to the system (2) can be

written as

$$\begin{aligned}\dot{x_i} &= f(x_i,y_i,z_i) + \frac{g_c}{k_c}(v_s - x_i)\sum_{j=1}^{N}\bar{\mathcal{A}}_{ij}^{(c)}\Gamma(x_j) \\ &\quad -\epsilon\sum_{j=1}^{N}\bar{\mathcal{L}}_{ij}^{(e)}x_j, \\ \dot{y_i} &= g(x_i,y_i,z_i), \\ \dot{z_i} &= h(x_i,y_i,z_i),\end{aligned} \tag{6}$$

where, $i = 1,2,\ldots,N$; $f(x,y,z) = y - ax^3 + bx^2 - z + I$, $g(x,y,z) = c - dx^2 - y, h(x,y,z) = r[s(x - x_0) - z], \Gamma(\mathbf{x}) = \frac{1}{1+\exp[\lambda(\Theta_s - \mathbf{x})]}$. Now we analyze the stability of the synchronized state of the above time-averaged system. Notice that each neural oscillator is identical in the time-averaged system and coupled by bidirectional electrical and chemical synapses. The evolution and interaction dynamics are both continuous and differentiable. So the stability criterion for synchronization can be found through the master stability function (MSF) formalism, which gives the necessary condition for stability of the synchronous solution. When synchronization occurs, let the network evolve synchronously with synchronization manifold $(x(t),y(t),z(t))$. If we perturb the ith node from the synchronization manifold by amount $(\delta x_i(t),\delta y_i(t),\delta z_i(t))$, then the current state at time t of the ith node will be $(x_i,y_i,z_i) = (x + \delta x_i, y + \delta y_i, z + \delta z_i)$. Considering small perturbations and expanding around the synchronous solution up to first order, we get linearized equations of the errors given by

$$\begin{aligned}\dot{\delta x_i} &= f_x\delta x_i + f_y\delta y_i + f_z\delta z_i - g_c\Gamma(x)\delta x_i - \epsilon\sum_{j=1}^{N}\bar{\mathcal{L}}_{ij}^{(e)}\delta x_j \\ &\quad + \frac{g_c}{k_c}(v_s - x)\Gamma_x(x)\left[k_c\delta x_i - \sum_{j=1}^{N}\bar{\mathcal{L}}_{ij}^{(c)}\delta x_j\right], \\ \dot{\delta y_i} &= g_x\delta x_i + g_y\delta y_i + g_z\delta z_i, \\ \dot{\delta z_i} &= h_x\delta x_i + h_y\delta y_i + h_z\delta z_i, \quad i = 1,2,\ldots,N.\end{aligned} \tag{7}$$

Of the $3N$ Lyapunov exponents of the above master stability equation (MSE), three are parallel to the synchronized manifold, and the remaining $(3N - 3)$ are transverse to that manifold. The transverse exponents determine the stability of the manifold, and to sort those out we project the error vector $(\delta x_i,\delta y_i,\delta z_i)$ onto the space spanned by the Laplacian eigenvectors $V^{(c)}$ of the average chemical synaptic layer. Since the Laplacian eigenvectors form a basis of $\mathbb{R}^N$, the choice of this layer is absolutely arbitrary. Let $(\xi_i^{(x)},\xi_i^{(y)},\xi_i^{(z)})$ be the projection of the synchronization error vector $(\delta x_i,\delta y_i,\delta z_i)$ onto the basis of eigenvectors. Then $(\xi_i^{(x)},\xi_i^{(y)},\xi_i^{(z)}) = (\sum_{j=1}^{N} V_{ij}^{(c)}\delta x_j, \sum_{j=1}^{N} V_{ij}^{(c)}\delta y_j, \sum_{j=1}^{N} V_{ij}^{(c)}\delta z_j)$. Obviously, this transformation of the error vector is a linear transformations (LT). Since $V^{(c)}$ is the matrix of eigenvectors which forms a basis of $\mathbb{R}^N$, the rank of these LT is N. Consequently, the kernel of this LT is the null space, which ensures that whenever synchronization error is zero, $(\xi_i^{(x)},\xi_i^{(y)},\xi_i^{(z)})$ becomes $(0,0,0)$, and vice versa. Now

$$\begin{aligned}\dot{\xi}_i^{(x)} &= \sum_{j=1}^{N} V_{ij}^{(c)}\dot{\delta x_j} \\ &= f_x\sum_{j=1}^{N} V_{ij}^{(c)}\delta x_j + f_y\sum_{j=1}^{N} V_{ij}^{(c)}\delta y_j + f_z\sum_{j=1}^{N} V_{ij}^{(c)}\delta z_j \\ &\quad -g_c\Gamma(x)\sum_{j=1}^{N} V_{ij}^{(c)}\delta x_j + g_c(v_s - x)\Gamma_x(x)\sum_{j=1}^{N} V_{ij}^{(c)}\delta x_j \\ &\quad -\frac{g_c}{k_c}(v_s - x)\Gamma_x(x)\sum_{j=1}^{N} V_{ij}^{(c)}\sum_{k=1}^{N}\bar{\mathcal{L}}_{jk}^{(c)}\delta x_k \\ &\quad -\epsilon\sum_{j=1}^{N} V_{ij}^{(c)}\sum_{k=1}^{N}\bar{\mathcal{L}}_{jk}^{(e)}\delta x_k.\end{aligned} \tag{8}$$

Each column $V_i^{(c)}$ is an eigenvector of $\bar{\mathcal{L}}^{(c)}$, i.e., $\sum_{j=1}^{N}\bar{\mathcal{L}}_{ij}^{(c)}V_{ij}^{(c)} = \gamma_i^{(c)}V_i^{(c)}$. So

$$\begin{aligned}\sum_{j=1}^{N} V_{ij}^{(c)}\sum_{k=1}^{N}\bar{\mathcal{L}}_{jk}^{(c)}\delta x_k &= \sum_{k=1}^{N}\sum_{j=1}^{N} V_{ij}^{(c)}\bar{\mathcal{L}}_{kj}^{(c)}\delta x_k \\ &= \sum_{k=1}^{N}\gamma_i^{(c)}V_{ik}^{(c)}\delta x_k = \gamma_i^{(c)}\xi_i^{(c)}.\end{aligned} \tag{9}$$

Let $V^{(e)}$ be the matrix of eigenvectors of $\bar{\mathcal{L}}^{(e)}$, the average Laplacian of the electrical synaptic network, with eigenvalue diagonal matrix $D^{(e)}$. Since Laplacian matrices are real symmetric, their eigenvectors are orthonormal, i.e., $V^{(c,e)}V^{(c,e)^T} = I_N$. This gives $\bar{\mathcal{L}}^{(e)}V^{(e)} = D^{(e)}V^{(e)}$, i.e., $\bar{\mathcal{L}}^{(e)} = V^{(e)}D^{(e)}V^{(e)^T}$, which implies $\bar{\mathcal{L}}_{ij}^{(e)} = \sum_{r=1}^{N} V_{ri}^{(e)}\gamma_r^{(e)}V_{rj}^{(e)}$.

Now $(\xi_1^{(x)},\xi_2^{(x)},\ldots,\xi_N^{(x)})^T = V^{(c)^T}(\delta x_1,\delta x_2,\ldots,\delta x_n)^T$ gives the projection of the synchronization error as

$$\delta x_k = \sum_{l=1}^{N} V_{lk}^{(c)}\xi_l^{(x)}. \tag{10}$$

Consider $U^{(e)} = V^{(e)^T}V^{(c)}$, which adequately captures the association of the Laplacian eigenvectors of the electrical synaptic layer with the chemical synapses and gives $U_{ij}^{(e)} = \sum_{k=1}^{N} V_{ik}^{(e)}V_{jk}^{(c)}$.

Then

$$\begin{aligned}\sum_{j=1}^{N} V_{ij}^{(c)}\sum_{k=1}^{N}\bar{\mathcal{L}}_{jk}^{(e)}\delta x_k &= \sum_{j=1}^{N}\sum_{k=1}^{N} V_{ij}^{(c)}\bar{\mathcal{L}}_{jk}^{(e)}\delta x_k \\ &= \sum_{j=1}^{N}\sum_{k=1}^{N}\sum_{r=1}^{N} V_{ij}^{(c)}V_{rj}^{(e)}\gamma_r^{(e)}V_{rk}^{(e)}\delta x_k \\ &= \sum_{j=1}^{N}\sum_{k=1}^{N}\sum_{r=1}^{N}\sum_{l=1}^{N} V_{ij}^{(c)}V_{rj}^{(e)}\gamma_r^{(e)}V_{rk}^{(e)}V_{lk}^{(c)}\xi_l^{(x)}\end{aligned}$$

$$= \sum_{r=1}^{N}\sum_{l=1}^{N}\left[\left\{\sum_{j=1}^{N} V_{ij}^{(c)} V_{rj}^{(e)}\right\}\gamma_r^{(e)}\left\{\sum_{k=1}^{N} V_{rk}^{(e)} V_{lk}^{(c)}\right\}\xi_l^{(x)}\right]$$

$$= \sum_{r=1}^{N}\sum_{l=1}^{N}\{U_{ri}^{(e)}\gamma_r^{(e)}U_{rl}^{(e)}\}\xi_l^{(x)}. \quad (11)$$

Using the results (9), (10), and (11) in (8),

$$\begin{aligned}\dot{\xi}_i^{(x)} &= f_x\xi_i^{(x)} + f_y\xi_i^{(y)} + f_z\xi_i^{(z)} - g_c\Gamma(x)\xi_i^{(x)} \\ &\quad + g_c(v_s - x)\Gamma_x(x)\xi_i^{(x)} - \frac{g_c}{k_c}(v_s - x)\Gamma_x(x)\gamma_i^{(c)}\xi_i^{(x)} \\ &\quad - \epsilon\sum_{r=1}^{N}\sum_{l=1}^{N} U_{ri}^{(e)}\gamma_r^{(e)}U_{rl}^{(e)}\xi_l^{(x)}. \end{aligned} \quad (12)$$

Now the two Laplacian matrices $\bar{\mathscr{L}}^{(e)}$ and $\bar{\mathscr{L}}^{(c)}$ commute with each other. So they have a common basis of eigenvectors, that is, $V^{(e)} = V^{(c)}$. Hence $U^{(e)} = I_N$ gives $U_{ij}^{(e)} = \delta_j^i$. Then projecting the error vector $(\delta x_i, \delta y_i, \delta z_i)$ onto the basis of eigenvectors, we can write MSE (7) as

$$\begin{aligned}\dot{\xi}_i^{(x)} &= f_x\xi_i^{(x)} + f_y\xi_i^{(y)} + f_z\xi_i^{(z)} - g_c\Gamma(x)\xi_i^{(x)} - \epsilon\gamma_i^{(e)}\xi_i^{(x)} \\ &\quad + \frac{g_c}{k_c}(v_s - x)\Gamma_x(x)\left[k_c\xi_i^{(x)} - \gamma_i^{(c)}\xi_i^{(x)}\right], \\ \dot{\xi}_i^{(y)} &= g_x\xi_i^{(x)} + g_y\xi_i^{(y)} + g_z\xi_i^{(z)}, \\ \dot{\xi}_i^{(z)} &= h_x\xi_i^{(x)} + h_y\xi_i^{(y)} + h_z\xi_i^{(z)}, \end{aligned} \quad (13)$$

for $i = 1,2,\ldots,N$. The direction of the eigenvector corresponding to eigenvalue 0 is parallel to the synchronization manifold, and the other eigenvectors are for transverse directions. So our required MSE transverse to the synchronization manifold can be written as

$$\begin{aligned}\dot{\xi}_i^{(x)} &= (-3ax^2 + 2bx)\xi_i^{(x)} + \xi_i^{(y)} - \xi_i^{(z)} \\ &\quad - \frac{g_c\xi_i^{(x)}}{1 + \exp[\lambda(\Theta_s - x)]} - \epsilon\gamma_i^{(e)}\xi_i^{(x)} + \frac{g_c}{k_c}(v_s - x) \\ &\quad \times \frac{\lambda\exp[\lambda(\Theta_s - x)]}{\{1 + \exp[\lambda(\Theta_s - x)]\}^2}\left[k_c\xi_i^{(x)} - \gamma_i^{(c)}\xi_i^{(x)}\right] \\ \dot{\xi}_i^{(y)} &= -2dx\xi_i^{(x)} - \xi_i^{(y)} \\ \dot{\xi}_i^{(z)} &= r\left(s\xi_i^{(x)} - \xi_i^{(z)}\right), \end{aligned} \quad (14)$$

where $i = 2,3,\ldots,N,(x,y,z)$ are the state variables of the synchronization manifold obeying

$$\begin{aligned}\dot{x} &= y - ax^3 + bx^2 - z + I + g_c(v_s - x)\Gamma(x) \\ \dot{y} &= c - dx^2 - y \\ \dot{z} &= r(s(x - x_0) - z). \end{aligned} \quad (15)$$

The maximum Lyapunov exponent (MLE) of the MSE given in Eq. (14), as a function of the parameter g_c and ϵ, gives the necessary condition for the stability of the synchronous solution. For the synchronous state to be stable, perturbation along all the transverse directions must die out, i.e., the values of MLE should be negative. When the least stable transversal mode associated with the eigenvalues λ_2 is stable, all other transversal modes remain stable. The variation of MLE of

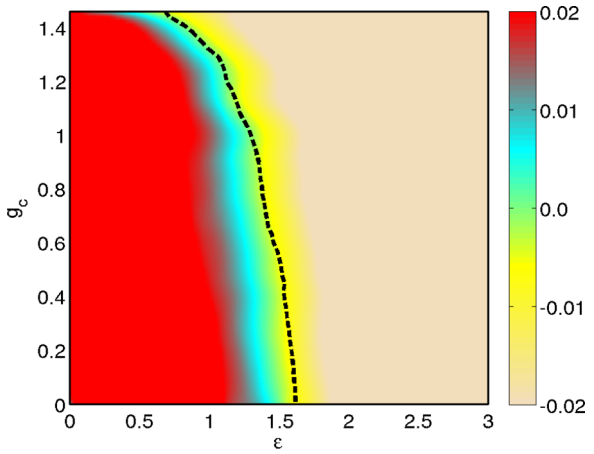

FIG. 11. The variation of the maximum Lyapunov exponent, denoted by the color bar, in the (ϵ, g_c) parameter space, for fixed $p = 0.1, k_c = 5, k_e = 6$. The corresponding analytical curve obtained using the Wu-Chua conjecture is shown by the black dashed line.

Eq. (14) is shown in the color-coded Fig. 11 in the parameter space of (ϵ, g_c). The synchronization error of the dynamic network for $f \in [10,100]$ vanishes approximately where the MLE becomes negative in Fig. 11; i.e., the MLE of the time-averaged network exactly matches with the time-varying network for sufficiently fast switching.

The Wu-Chua conjecture [55] gives a relation between the eigenvalues of Laplacian matrix and synchronization threshold in network of various sizes for linearly coupled dynamical systems. This states that for a network of linearly coupled dynamical systems, if the synchronization threshold for a network of size N is ϵ_N^*, and the synchronization threshold for a network of size n is ϵ_n^*, then

$$\epsilon_N^*\gamma_2(N) = \epsilon_n^*\gamma_2(n), \quad (16)$$

where $\gamma_2(N)$ and $\gamma_2(n)$ are the smallest nonzero eigenvalues of the Laplacian matrix for network size N and n, respectively. This suggests that if we choose $n = 2$, then we can predict the synchronization threshold for a network of any arbitrary size N, by simply studying the synchronization of two coupled systems, as $\epsilon_N^* = \frac{2\epsilon_2^*}{\gamma_2(N)}$.

Now for our case, the dynamics of the membrane potential of the ith neuron for a time-averaged network can be written as

$$\dot{x}_i = f(x_i, y_i, z_i) + \frac{g_c}{N-1}(v_s - x_i)\sum_{j\neq i}\Gamma(x_j) - \epsilon\sum_{j=1}^{N}\bar{\mathscr{L}}_{ij}^{(e)}x_j. \quad (17)$$

Apparently the nonlinear coupling term acts as a global chemical synaptic coupling with strength $\frac{g_c}{N-1}$. So from Ref. [56], in the absence of electrical synapses, the synchronization threshold for the nonlinear coupling obeys

$$g_c^{(N)*} = g_c^{(2)*}, \quad (18)$$

where $g_c^{(N)*}$ is the critical value of g_c for N neurons; i.e., the chemical synaptic strength has no N-dependent effect on the synchronization threshold. But from the Wu-Chua conjecture the electrical coupling definitely has a N-dependent effect

at the transition point. So the synchronization threshold of electrical coupling as a function of g_c, in terms of the critical values for two electrically and chemically coupled neurons, is given as

$$\epsilon_N^*(g_c) = \frac{2\epsilon_2^*(g_c)}{\gamma_2^{(e)}(N)}, \tag{19}$$

where $\epsilon_N^*(g_c)$ and $\epsilon_2^*(g_c)$ are the critical electric coupling strengths for given a g_c for network size N and 2, respectively. Let $\gamma_2^{(e)}(N)$ be the lowest nonzero eigenvalues of the time-averaged Laplacian matrices corresponding to the electrical synaptic network of size N. For different values of g_c we obtained the critical value of the electrical coupling strength $\epsilon_N^*(g_c)$, considering the other parameters to be the same as those in Fig. 11. This analytical curve is plotted with a black dashed line in Fig. 11, with the parameter regions above and below the transition line corresponding to the synchronized and desynchronized states. It is clearly seen to be in excellent agreement with the results obtained through the MSF formalism, and this lends further support to the Wu-Chua conjecture as well.

V. EFFECTS OF THE REWIRING FREQUENCY ON FIRING REGULARITY

In this section, we investigate how rewiring frequency affects firing regularity of the individual neurons in the network. Inspecting the distribution of the interspike interval (ISI) is considered one of the best ways to quantify the degree of regularity in spiking patterns, that is, the distribution of the time between two consecutive spikes, for sufficiently long spike sequences. Let $F_i(x)$ be the distribution of the ISI of the ith neuron, where $\int_{t_0}^{t_0+s} F_i(x)\,dx$ is the probability of occurrence of next spike of the ith neuron in the interval $[t_0, t_0+s]$, given that the last spike occurred at time t_0. Then the mean firing interval of the ith neuron is denoted as $\langle s_i \rangle$ and defined as

$$\langle s_i \rangle = \int_0^\infty x F_i(x)\,dx. \tag{20}$$

The CV_i of the ith neuron is the ratio of the standard deviation and the mean, which quantifies the width of the interval distribution:

$$\mathrm{CV}_i = \frac{\sqrt{\int_0^\infty x^2 F_i(x)\,dx - \langle s_i \rangle^2}}{\langle s_i \rangle}. \tag{21}$$

If $\mathrm{CV}_i = 1$, then the spike train will follow a Poisson-like process, while a more regular firing pattern yields CV_i less than 1, with CV_i becoming zero if the ith neuron fires periodically. So CV_i indicates the deviation of the spike sequence from a random Poisson process. The mean firing interval of the ith neuron is estimated as $\langle s_i \rangle = \frac{1}{M_i}\sum_{j=1}^{M_i}(t_{j+1} - t_j)$ and the mean-square deviation of ISIs, as $\frac{1}{M_i}\sum_{j=1}^{M_i}(t_{j+1} - t_j)^2$, where t_j is the time of the jth spike and M_i is the total number of spikes in the spike sequence of the ith neuron. So,

$$\mathrm{CV}_i = \frac{\sqrt{\frac{1}{M_i}\sum_{j=1}^{M_i}(t_{j+1} - t_j)^2 - \langle s_i \rangle^2}}{\langle s_i \rangle}. \tag{22}$$

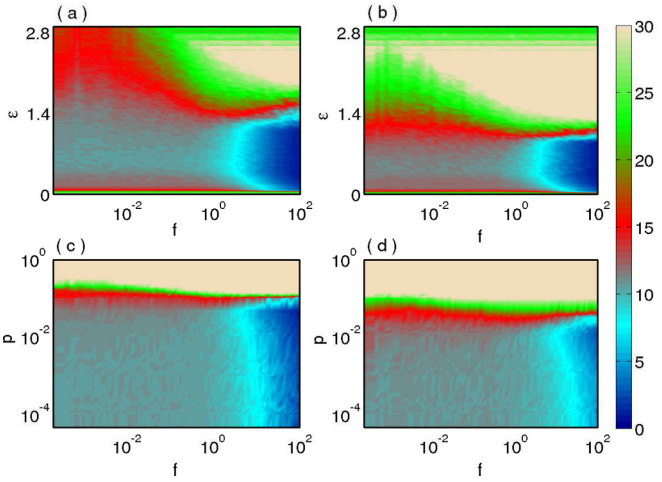

FIG. 12. Variation of the interspike interval (ISI) in the parameter space of (upper row) rewiring frequency f and coupling strength ϵ, for fixed $p = 0.1$ and average degree (a) $k_e = 4$ and (b) $k_e = 6$, and (lower row) rewiring frequency f and p, for fixed values of $k_e = 6$ and (c) $\epsilon = 1.0$ and (d) $\epsilon = 2.0$. Here $g_c = \frac{\epsilon}{2}$. Note that the coupling strengths are such that the states in (c) are desynchronized, while the states in (d) are synchronized.

Now to gauge the firing regularity of the full neuronal network, the mean ISI and the CV of the network are estimated as $\langle s \rangle = \frac{1}{N}\sum_{i=1}^{N}\langle s_i \rangle$ and $\mathrm{CV} = \frac{1}{N}\sum_{i=1}^{N}\mathrm{CV}_i$. Smaller values of CV correspond to higher firing regularity and a more ordered spiking pattern in the entire network.

Figure 12 shows the ISI in different regions of parameter space. The upper panels in the figure display the variation of ISI in the parameter space of synaptic coupling strength and the rewiring frequency f, while the lower panels display the variation of ISI in the parameter space of the small-world probability p and f. We find that for small average degree [such as in the illustrative example of $k_e = 4$ in Fig. 12(a)] the average time interval between spikes is large only in the synchronization region of parameter space [cf. Fig. 2(a)], while the time interval between consecutive firings is small for desynchronized states. However, for larger average degree [such as $k_e = 6$ in Fig. 12(b)], large ISI occurs for synchronized states as well as a desynchronized one. Further we see that *rapidly varying networks yield rapid spiking*, i.e., high f gives rise to small ISI. We also see that a *more random network yields more infrequent spiking*, i.e., the limit of $p \to 1$ gives rise to very high ISI, irrespective of the value of f, for both desynchronized states [Fig. 12(c)] and synchronized states [Fig. 12(d)]. One can also see that the critical value of p after which ISI becomes large and independent of f is larger for the desynchronized state [Fig. 13(c)], as compared to the synchronized state [Fig. 13(d)] where this transition occurs at lower values of p.

Next we estimate the irregularity of the spiking pattern of the neurons by computing CV (i.e., the ratio of the standard deviation and the mean of the ISI distribution) corresponding to the ISI data shown in Fig. 12. Figure 13 shows this measure. It is clear that the firing patterns are more regular in the synchronized regions as the value of CV is much less than 1 there, as compared to that in the desynchronized regions. Further

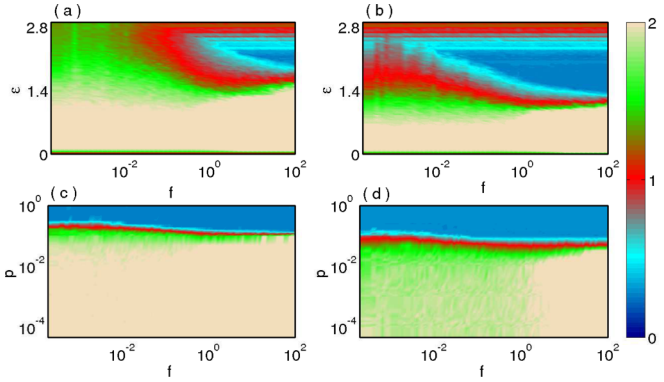

FIG. 13. Variation of CV in the parameter space (as in Fig. 12) of (upper row) rewiring frequency f and coupling strength ϵ, for fixed $p = 0.1$ and average degree (a) $k_e = 4$ and (b) $k_e = 6$, and (lower row) rewiring frequency f and p, for fixed values of $k_e = 6$ and (c) $\epsilon = 1.0$ and (d) $\epsilon = 2.0$. Here $g_c = \frac{\epsilon}{2}$. Again note that the coupling strengths are such that the states in (c) are desynchronized, while the states in (d) are synchronized.

the *spike trains are more regular in synaptic networks of higher average degree* [cf. Fig. 13(a) *vis-à-vis* Fig. 13(b)]. For networks with lower average degree [e.g., $k_e = 4$ in Fig. 13(a)] the spike train follows the Poisson process (as CV ≈ 1) up to a certain threshold value of f. However, for higher average degree [e.g., $k_e = 6$ in Fig. 13(b)] the firing is consistent with a Poisson process for lower link-switching frequencies (close to the static case), and after a critical value of coupling strength the CV follows the Poisson process irrespective of rewiring frequency f. Further, interestingly, after a critical value of the small-world probability ($p \sim 0.1$) regular spike train patterns are observed, independent of the network rewiring frequency f. That is, *more random networks yield more regular firing, regardless of the time-varying nature of the links*, for both desynchronized states [Fig. 13(c)] and synchronized states [Fig. 13(d)]. Additionally, when the neurons in the network are firing synchronously [e.g., for $\epsilon = 2, g_c = 2.0$ as shown in Fig. 13(d)], then periodic spiking occurs for a larger range of p, i.e., the onset of regular spike trains arises at lower critical values of p.

VI. CONCLUSIONS

We have presented a general mathematical framework of time-varying hypernetworks i.e., a network with two distinct coexisting network topologies and interaction functions, and explored the emergence of synchrony. In order to illustrate the broad ideas, we focused on a particular model mimicking neuronal networks i.e., time-varying hypernetworks of Hindmarsh-Rose model neurons with two distinct types of synaptic communications. In our proposed network, the neurons interact through electrical synapses (i.e., gap junctional coupling), as well as through chemical synapses. As the electrical interaction is bidirectional and the chemical interaction is unidirectional, we have considered a hypernetwork consisting of two different types of network topologies. The first is a bidirectional gap junctional coupling on a small-world network, and the other is a unidirectionally coupled random network associated with the chemical coupling. Further, in this work we went beyond a hypernetwork with static links and considered both synaptic networks to be time-varying, with the links changing stochastically with a characteristic rewiring frequency f. We found that the coupling strength necessary to achieve complete neuronal synchrony is lower when the links are switched rapidly. This implies that more rapidly changing networks yield larger windows of complete synchronization in the parameter space of electrical and chemical coupling strengths. Further, the average time required to reach the synchronized state decreases as synaptic coupling strength and/or rewiring frequency increases. We also investigated the resilience of the synchronous states with respect to increasing network size. We found that, while increasing network size induces desynchronization, synchrony can be maintained up to larger network sizes by increasing either synaptic strength or rewiring frequency.

Next we analyzed the local stability of the synchronous state adopting the master stability function approach for the time-averaged system, which closely mimics the hypernetwork when the links are switched rapidly. Using the Wu-Chua conjecture, we analytically derived the critical transition to stable synchronous states and found excellent agreement with our numerical results. We further probed the global stability of the network through the basin stability measure. This again showed that faster rewiring and stronger coupling aided the global stability of the synchronous state. Further, for fast changing connections there was a sharper transition from the incoherent to the synchronous state, and the region of coexistence of the synchronous and desynchronous states decreases as rewiring frequency increases.

Last, we found that time-varying links not only promote complete synchronization, but also have the capacity to change the local dynamics of each single neuron. We found that rapidly varying networks yield rapid spiking; i.e., high f gives rise to small interspike interval (ISI). We also found that a more random network (i.e., with higher p) yields more infrequent, but more regular, spike trains. Further, we observed that the spiking behavior becomes more regular in synaptic networks of higher average degree. So our findings on the effect of the structure and temporal variation of synaptic links on collective synchrony, as well as local spiking dynamics, can potentially lead to better understanding of complex neuronal hypernetworks that interact through different channels.

Finally, we expect that this study will broaden our understanding of different collective behavior in time-varying hypernetworks. Our results on synchrony in the multilayer structure of temporal hypernetworks should hold considerable relevance and find potential applications in other hypernetwork models of physical, biological, sociological, and engineered phenomena. So our broad results here may trigger further research on some of the open questions arising from this work, as well as exploration of more realistic models in the future.

ACKNOWLEDGMENTS

D.G. was supported by SERB-DST (Department of Science and Technology), Government of India (Project No. EMR/2016/001039). The authors acknowledge the anonymous referees for their insightful suggestions.

[1] F. Sorrentino, New J. Phys. **14**, 033035 (2012).
[2] P. J. Mucha, T. Richardson, K. Macon, M. A. Porter, and J. P. Onnela, Science **328**, 876 (2010).
[3] S. V. Buldyrev, R. Parshani, G. Paul, H. E. Stanley, and S. Havlin, Nature (London) **464**, 1025 (2010).
[4] M. Kurant and P. Thiran, Phys. Rev. Lett. **96**, 138701 (2006).
[5] C. Zhou, L. Zemanova, G. Zamora, C. C. Hilgetag, and J. Kurths, Phys. Rev. Lett. **97**, 238103 (2006); New J. Phys. **9**, 178 (2007).
[6] B. L. Partridge and T. J. Pitcher, J. Comput. Physiol. **135**, 315 (1980).
[7] N. Abaid and M. Porfiri, J. R. Soc. Interface **7**, 1441 (2010).
[8] M. S. Baptista, F. M. Moukam Kakmeni, and C. Grebogi, Phys. Rev. E **82**, 036203 (2010).
[9] E. M. Izhikevich, *Dynamical Systems in Neuroscience: The Geometry of Excitability and Bursting* (MIT Press, Cambridge, MA, 2007).
[10] D. Irving and F. Sorrentino, Phys. Rev. E **86**, 056102 (2012).
[11] R. Sevilla-Escoboza, R. Gutiérrez, G. Huerta-Cuellar, S. Boccaletti, J. Gómez-Gardeñes, A. Arenas, and J. M. Buldú, Phys. Rev. E **92**, 032804 (2015).
[12] M. Komarov and A. Pikovsky, Phys. Rev. E **92**, 020901(R) (2015).
[13] N. B. Ouchi and K. Kaneko, Chaos **10**, 359 (2000).
[14] C. I. Del Genio, J. Gómez-Gardeñes, I. Bonamassa, and S. Boccaletti, Sci. Adv. **2**, e1601679 (2016).
[15] P. Holme and J. Saramäki, Phys. Rep. **519**, 97 (2012).
[16] S. Wasserman and K. Faust, *Social Network Analysis: Methods and Applications* (Cambridge University Press, Cambridge, 1994).
[17] R. Pastor-Satorras and A. Vespignani, *Evolution and Structure of the Internet: A Statistical Physics Approach* (Cambridge University Press, Cambridge, 2004).
[18] I. V. Belykh, V. N. Belykh, and M. Hasler, Physica D **195**, 188 (2004).
[19] S. Rakshit, S. Majhi, B. K. Bera, S. Sinha, and D. Ghosh, Phys. Rev. E **96**, 062308 (2017).
[20] A. Mondal, S. Sinha, and J. Kurths, Phys. Rev. E **78**, 066209 (2008).
[21] J. Lü and G. Chen, IEEE Trans. Autom. Control **50**, 841 (2005).
[22] M. Frasca, A. Buscarino, A. Rizzo, L. Fortuna, and S. Boccaletti, Phys. Rev. Lett. **100**, 044102 (2008).
[23] S. Majhi and D. Ghosh, Chaos **27**, 053115 (2017).
[24] D. Levis, I. Pagonabarraga, and A. Díaz-Guilera, Phys. Rev. X **7**, 011028 (2017).
[25] R. Olfati-Saber, J. A. Fax, and R. M. Murray, Proc. IEEE **95**, 215 (2007).
[26] V. Kohar and S. Sinha, Chaos, Solitons, Fractals **54**, 127 (2013).
[27] M. Valencia, J. Martinerie, S. Dupont, and M. Chavez, Phys. Rev. E **77**, 050905(R) (2008).
[28] M. L. Sachtjen, B. A. Carreras, and V. E. Lynch, Phys. Rev. E **61**, 4877 (2000).
[29] J.-P. Onnela, J. Saramaki, J. Hyvonen, G. Szabo, D. Lazer, K. Kaski, J. Kertesz, and A. L. Barabasi, Proc. Natl. Acad. Sci. USA **104**, 7332 (2007).
[30] D. Tanaka, Phys. Rev. Lett. **99**, 134103 (2007).
[31] F. Sivrikaya and B. Yener, IEEE Netw. **18**, 45 (2004).
[32] T. M. Przytycka, M. Singh, and D. K. Slonim, Briefings Bioinf. **11**, 15 (2010); S. Lébre, J. Becq, F. Devaux, M. P. H. Stumpf, and G. Lelandais, BMC Syst. Biol. **4**, 130 (2010); A. Rao, A. O. Hero, D. J. States, and J. D. Engel, EURASIP J. Bioinform. Syst. Biol. **2007**, 51947 (2007).
[33] F. de Vico Fallani, V. Latora, L. Astolfi, F. Cincotti, D. Mattia, M. G. Marciani, S. Salinari, A. Colosimo, and F. Babiloni, J. Phys. A **41**, 224014 (2008).
[34] D. S. Bassett, N. F. Wymbs, M. A. Porter, P. J. Mucha, J. M. Carlson, and S. T. Grafton, Proc. Natl. Acad. Sci. USA **108**, 7641 (2011).
[35] D. S. Bassett and Ed Bullmore, Neuroscientist **12**, 512 (2006).
[36] D. S. Bassett and E. T. Bullmore, Neuroscientist **23**, 499 (2017).
[37] C. C. Hilgetag and A. Goulas, Brain Struct. Funct. **221**, 2361 (2016).
[38] P. J. Menck, J. Heitzig, N. Marwan, and J. Kurths, Nat. Phys. **9**, 89 (2013).
[39] S. Leng, W. Lin, and J. Kurths, Sci. Rep. **6**, 21449 (2016).
[40] S. Rakshit, B. K. Bera, S. Majhi, C. Hens, and D. Ghosh, Sci. Rep. **7**, 45909 (2017).
[41] V. Kohar, P. Ji, A. Choudhary, S. Sinha, and J. Kurths, Phys. Rev. E **90**, 022812 (2014).
[42] S. Rakshit, B. K. Bera, M. Perc, and D. Ghosh, Sci. Rep. **7**, 2412 (2017).
[43] C. Meena, K. Murali, and S. Sinha, Int. J. Bif. Chaos **26**, 1630023 (2016).
[44] S. G. Hormuzdi, M. A. Filippov, G. Mitropoulou, H. Monyer, and R. Bruzzone, Biochim. Biophys. Acta **1662**, 113 (2004).
[45] E. R. Kandel, J. H. Schwartz, and T. M. Jessell, *Principles of Neural Science* (McGraw-Hill, New York, USA, 2000).
[46] A. E. Pereda, Nat. Rev. **15**, 250 (2014).
[47] X. Liao, A. V. Vasilakos, and Y. He, Neurosci. Biobehav. Rev. **77**, 286 (2017).
[48] D. S. Bassett, A. Meyer-Lindenberg, S. Achard, T. Duke, and E. Bullmore, Proc. Natl. Acad. Sci. USA **103**, 19518 (2006).
[49] S. F. Muldoon, E. W. Bridgeford, and D. S. Bassett, Sci. Rep. **6**, 22057 (2016).
[50] D. J. Watts and S. H. Strogatz, Nature (London) **393**, 440 (1998).
[51] S. Sinha, Phys. Rev. E **66**, 016209 (2002).
[52] P. M. Gade and S. Sinha, Phys. Rev. E **72**, 052903 (2005).
[53] M. P. K. Jampa, A. R. Sonawane, P. M. Gade, and S. Sinha, Phys. Rev. E **75**, 026215 (2007).
[54] D. J. Stilwell, E. M. Bollt, and D. G. Roberson, SIAM J. Appl. Dyn. Syst. **5**, 140 (2006).
[55] C. W. Wu and L. O. Chua, IEEE Trans. Circuits Syst.-I **43**, 161 (1996).
[56] I. Belykh, E. de Lange, and M. Hasler, Phys. Rev. Lett. **94**, 188101 (2005).